



## RESEARCH ARTICLE

PLASMA PROCESSES  
AND POLYMERS

# Surface modification of recycled polymers in comparison to virgin polymers using Ar/O<sub>2</sub> plasma etching

Martin Amberg<sup>1</sup>  | Marion Höhener<sup>1</sup> | Patrick Rupper<sup>1</sup> |  
Barbara Hanselmann<sup>1</sup> | Rudolf Hufenus<sup>1</sup> | Sandro Lehner<sup>1</sup> | Edith Perret<sup>1,2</sup> |  
Dirk Hegemann<sup>1</sup> 

<sup>1</sup>Laboratory for Advanced Fibers, Empa, Swiss Federal Laboratories for Materials Science and Technology, St. Gallen, Switzerland

<sup>2</sup>Center for X-ray Analytics, Empa, Swiss Federal Laboratories for Materials Science and Technology, Dübendorf, Switzerland

## Correspondence

Martin Amberg, Empa, Swiss Federal Laboratories for Materials Science and Technology, Lerchenfeldstrasse 5, 9014 St. Gallen, Switzerland.

Email: [martin.amberg@empa.ch](mailto:martin.amberg@empa.ch)

## Funding information

Innosuisse - Schweizerische Agentur für Innovationsförderung,  
Grant/Award Number: 12404.1 PFIW-IW

## Abstract

Low-pressure plasma etching of a recycled polyethylene terephthalate (PET) film is studied in comparison to virgin PET and polypropylene (PP) using a capacitively coupled radio frequency (RF) plasma reactor. Recycled polymers are distinguished by increased impurity content and weakened mechanical properties, both affecting plasma etching and adhesion processes. Mild plasma conditions have been selected to maintain the material bulk properties of the polymers. The etch rates and the morphology of the polymer samples were thus determined at floating potential compared with etching at the RF electrode for varying argon/oxygen gas mixtures, etching duration, and sample size. Thermoanalytical and X-ray techniques were used to characterize the polymer before and after the plasma etching treatment. Finally, adhesive-tape peel tests proved that excellent adhesion of silver coatings can also be achieved on a plasma-treated recycled PET film.



## KEYWORDS

adhesion promotion, floating potential, plasma etching, polymer morphology, recycling effects

This is an open access article under the terms of the Creative Commons Attribution-NonCommercial License, which permits use, distribution and reproduction in any medium, provided the original work is properly cited and is not used for commercial purposes.

© 2022 The Authors. *Plasma Processes and Polymers* published by Wiley-VCH GmbH.

## 1 | INTRODUCTION

The extraordinary material properties of synthetic polymers stem from their macromolecules (polymer architecture and chain length), their morphology (polymer chain interaction and crystallinity), and their additives (organic and inorganic compounds). All three influence the susceptibility of a polymer to plasma etching, for example, due to chain scission.<sup>[1,2]</sup> As a consequence of the ever-increasing plastic waste and related issues, the use of recycled polymer material is an urgent demand of our society, whereby quality requirements for the secondary material need to be fulfilled.<sup>[3]</sup> The growing importance of thermo-mechanical recycling of polymers, however, results in weakened mechanical properties of the recycled material, typically related to residual contaminants, a lower molecular weight due to chain scission mechanisms, formation of oligomers, and amorphous chain defects.<sup>[4–7]</sup> Impurities, chain ends, branches, and interfaces of crystalline-amorphous fractions can act as traps for ions accelerated by the plasma to the polymer surface, which influence the momentary surface modification.<sup>[8]</sup> However, only a few studies report on the plasma modification of recycled polymers, while it can be assumed that differences compared with virgin polymers might also affect adhesion.<sup>[9–11]</sup>

Reports on low-pressure plasma etching of organic polymers are going back to the beginning of lithography for removing photoresists on integrated circuits<sup>[12]</sup> as has been summarized by Oehrlein.<sup>[2]</sup> The photoresist stripping is performed in reactive ion etching (RIE) batch processes, where it is common to place the sample directly on the RF-driven electrode to gain high etch rates by using halogen gases.<sup>[13]</sup> The plasma contains charged particles (ions and electrons), excited neutrals, radicals, and ultraviolet (UV) radiation,<sup>[14–16]</sup> which can react with a polymeric surface to remove contaminations, introduce chemical functionalities, and induce chain scission and cross-linking.<sup>[1,14,17]</sup>

By energy-flux density measurement, the etch-rate determining mechanism of Ar and O<sub>2</sub> RIE was found to strongly depend on the bombardment of energetic particles.<sup>[18]</sup> In addition, reactions with oxygen radicals usually yield carbonyl, hydroxyl, or carboxylic acid groups on the sample surface. These findings have been used in the plastics industry to induce a surface topography sufficient to enable printing operations<sup>[14,19]</sup> and other applications involving adhesives, coatings, composites, and electronics. Immediately after oxygen plasma treatment, the polymer surfaces show superhydrophilicity, due to a combined effect of surface oxidation and enhanced roughness of the surface.<sup>[20–22]</sup> Although induced roughness and crosslinking

by plasma etching are irreversible changes, the hydrophobic character of polymers, however, is largely restored during aging due to thermodynamically driven restructuring, leaching of low-molecular-weight oxidized materials (LMWOM), and compensation of trapped charges.<sup>[8]</sup>

Etch rates typically increase with oxygen atom concentration in the plasma.<sup>[18,23]</sup> The highest etch rates involved pure oxygen followed by air, nitrogen, and argon gases.<sup>[24]</sup> Enhanced etch rates are also observed for polymers containing a high fraction of oxygen with a related high Ohnishi parameter of the polymer,<sup>[25]</sup> whereas structures containing benzene rings are more resistant to oxidation and etching.<sup>[1]</sup> Plasma exposure also causes the loss of C–H bonds as a result of hydrogen abstraction.<sup>[26]</sup> Chain scission leads to a surface rich in LMWOM, which are either removed via the vacuum system or remain on the surface.<sup>[27]</sup> Etching and chemical modification often occur simultaneously and are competitive processes that also depend on gas pressure.<sup>[17]</sup>

Vesel and Semenik examined an inductively coupled reactive plasma on polyethylene terephthalate (PET) (amorphous and semi-crystalline), polymethylmethacrylate, polystyrenePS, low density polyethylene, high density polyethylene, polyvinyl chloridePVC, and polytetrafluoroethylene, observing no difference in etch rates for amorphous and semi-crystalline PET.<sup>[28]</sup> Other studies, however, stated differences in etch rates related to crystallinity, since chain scission is more pronounced in amorphous polymers.<sup>[25]</sup> Investigations by Xie et al. showed an increase of crystallinity with O<sub>2</sub>/Ar plasma treatment time of PET films at 60 W RF power related to the preferred etching of amorphous phases and heat load.<sup>[29]</sup>

An increased etch rate above the glass transition temperature was observed for photoresists by Pons<sup>[30]</sup> and for PET by Krstulovic.<sup>[31]</sup> It has been coincidentally reported that crystalline phases can be observed by scanning electron microscopy (SEM) and scanning force microscopy investigations.<sup>[17,21]</sup> Fischer et al. reported SEM-derived surface roughness data showing that while oxygen plasma roughens the surface, argon plasma does less.<sup>[32]</sup> Heather et al. found a fibrillary structure on O<sub>2</sub> RIE-etched PET samples and less for Ar plasma conditions.<sup>[33]</sup>

The above-mentioned experiments and studies were mainly performed in RIE systems where the samples are treated on the RF-driven electrode. Less studies considered plasma etching conditions with samples placed electrically insulated (floating) in the active plasma zone without contact to the driven RF electrode or grounded wall as etch rates are lowered in this case. Holland and

Ojha observed reduced etch rates at floating conditions by a factor of 4 compared with the sample placed on the RF electrode with a negative bias of 500 V.<sup>[34]</sup> The electrical floating potential held by an insulated sample,  $V_f$ , is established by an equal flux of positive and negative species. To maintain this equal flux,  $V_f$  is typically around 10–20 V depending on electron temperature. This lower voltage drop across the floating sheath yield less acceleration of ions accompanied by lower etch rates compared with samples placed directly at the RF electrode with a high bias voltage. The role of ion energies and ion flux under floating conditions was investigated in more detail by Trieschmann and Hegemann.<sup>[35]</sup>

Hence, etching conditions are milder yielding a lower heat load for floating samples and therefore less damaging to the polymer, especially for thin specimens. As an example, the tensile strength of PET fibers could be retained under such conditions, whereas increased heat load resulted in lowered mechanical properties.<sup>[36]</sup> For this reason, plasma etching at floating conditions can be advantageous despite lowered etch rates.<sup>[37]</sup>

The aim of this article is thus to study the plasma etching processes of two polymer materials, PET (virgin and recycled films) and polypropylene (PP) (film and injection-molded cup), which are among the most common polymer types. All four polymer materials are commercially used for packaging. These polymers were plasma-treated at floating potential using conditions that maintain the material properties such as the bulk crystallinity. Furthermore, the plasma treatment at floating conditions might simplify the etching process for roll-to-roll (R2R) treatment of fibers and web material, or generally for polymer films that have to be treated on both sides. As an example, the achievement of industrially relevant adhesion forces of a silver coating deposited by sputtering on plasma-etched recycled PET (rPET) is demonstrated allowing R2R processing.

## 2 | METHODS

### 2.1 | Plasma reactor, parameters, and sample positioning

Plasma etching was carried out at low pressure within a highly asymmetric, capacitively coupled radiofrequency (RF) batch reactor (13.56 MHz) consisting of a DN ISO-K 160 T-piece schematically shown in Figure 1 and is described in more detail elsewhere.<sup>[20,35]</sup> The vacuum system was composed of a rotary pump and a turbo pump generating a base pressure in the  $10^{-4}$  Pa range.

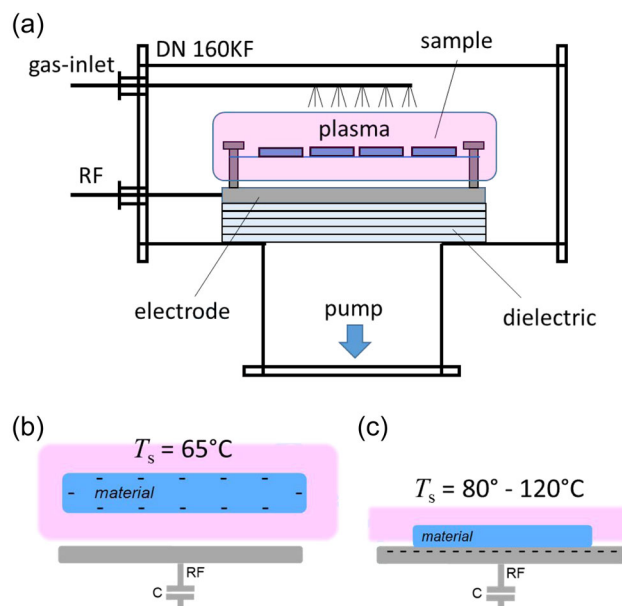


**FIGURE 1** Plasma reactor setup shown in (a) with the radio frequency (RF)-driven electrode placed in the center of the ISO DN 160 T-piece indicating the position of floating samples 2 cm above the electrode with a suspension system. The placement of the sample is shown in simplified form in (b) yielding negative charging of the entire polymer surface at floating conditions. In contrast, ion etching with the samples placed on the electrode is shown in (c). Temperatures refer to measured sample temperatures  $T_s$ .

The pressure was measured by a Baratron pressure gauge (MKS Instruments) and adjusted by a throttling valve (VAT). The gas flow rates were controlled via mass flow controllers (MKS) and let into the vacuum chamber by a shower head 6 cm above the electrode. The RF-driven aluminum electrode ( $10 \times 15 \text{ cm}^2$ ) in the center of the vacuum chamber was insulated by five sheets of glass each 4 mm thick (as dielectric) from the grounded chamber walls.

The polymer samples consisted of a PET film (Mylar 12HP, DuPont) of  $15 \mu\text{m}$  thickness, and an recycled PET (rPET 200  $\mu\text{m}$  thick film (B130BOXX, Folientechnik), and PP in the form of a  $60 \mu\text{m}$  thick film, and an injection-molded cup (Greiner Packaging). All samples were provided without color additives, that is, in the transparent state. From the injection-molded PP cups the bottom part ( $\varnothing 30 \text{ mm}$ , thickness of  $600 \mu\text{m}$ ) was taken to obtain flat samples. The samples were placed at floating conditions 2 cm above the electrode (Figure 1b) by means of a suspension system similar to a clothesline or directly on the RF electrode (Figure 1c) for reference. The plasma etching was performed with 30 W, 4 Pa at a total flow rate of 20 sccm (Ar or  $\text{O}_2$  or mixture) and 7.5 min of treatment time unless otherwise specified.

The sample temperature  $T_S$  was measured during the plasma treatment by an iButton DS1922T-F5 (Maxim Integrated) temperature logger at the electrode and at a floating potential. Due to the higher thermal mass of the temperature logger compared with the polymer films,  $T_S$  was recorded until a steady state was reached. Generally, all polymers were used as received, except for one comparative study using rPET samples that were additionally annealed in an oven at 160° for 10 min. The luminosity distribution in the visible range of the plasma above the RF electrode was observed using a digital camera (Nikon CoolPix 5700) at fixed camera settings (lens aperture 7.4, exposure time 0.5 s) and constant surrounding conditions to obtain comparable relative intensities.<sup>[38,39]</sup>

## 2.2 | Determination of etch rates

The samples were dried in a vacuum ( $3 \times 10^{-3}$  Pa) for at least 12 h. After drying they were weighted by a microbalance (Mettler-Toledo, Type XS204) with 0.1 mg accuracy. The measurements were performed in 23°C/50% relative humidity until the mass of the samples was constant within  $\pm 0.1$  mg. Only rPET showed a noticeable moisture absorption of 0.4% by weight. The influence of plasma on moisture uptake was measured in a dry and conditioned state.

The average etch rate of the flat polymer samples placed at the electrode or at floating conditions was calculated as follows:

$$R = \frac{\Delta m}{\rho \cdot A \cdot t}, \quad (1)$$

where  $\Delta m$  is the weight loss in [g],  $\rho$  is the density (PET: 1.335 and PP: 0.91 g cm<sup>-3</sup>),  $t$  the process time, and  $A$  is the etched area in [cm<sup>2</sup>] exposed to the plasma. The samples are denominated by “-e” and “-f” for samples treated on the electrode and at floating conditions, respectively. For floating samples the front and backside are both treated, therefore twice the sample size was taken for the calculation of the average etch rate. The standard deviation was calculated from at least four samples for each polymer.

For determining the individual etch rate for floating samples facing the electrode and opposite side (see the experiment in Section 3.4), two polymer films were tightly piled on top of each other and treated by plasma etching the same way as single films. The etch rate was then calculated with the area of one single side.

## 2.3 | Polymer and structural analytics

Differential scanning calorimetry (DSC) was performed with a DSC 214 device (NETZSCH-Gerätebau GmbH). For each sample 5 mg was used and the initial heating curves were performed with 10 K min<sup>-1</sup>. From DSC curves the crystallinity,  $W_c$ , was calculated by the following formula:

$$W_c = \frac{\Delta H_m - \Delta H_c}{\Delta H}, \quad (2)$$

where  $\Delta H_c$  is the cold crystallization enthalpy and  $\Delta H_m$  the enthalpy of melting, and  $\Delta H$  is the enthalpy of theoretically fully crystallized PET (140 Jg<sup>-1</sup>) and PP (207 Jg<sup>-1</sup>), respectively.<sup>[40,41]</sup>

Wide-angle x-ray diffraction (WAXD) patterns were recorded using a Cu-K $\alpha$  source ( $\lambda = 1.5419$  Å) on a Bruker Nanostar U diffractometer (Bruker AXS). The X-rays were sent through a beam-defining pinhole of 300  $\mu$ m onto the samples, which have been mounted on a frame and the sample to detector distance was 9.4 cm. A VÅNTEC-2000 MikroGap served as an area detector.

Gel permeation chromatography (GPC) was used to determine the molecular weight of recycled and virgin PET and of an amorphous PET reference sample.

## 2.4 | Surface analytics

Morphological surface investigations have been performed on the untreated as well as etched samples using a scanning electron microscope (SEM) (Hitachi S-4800). For each sample, the SEM analysis was performed in various randomly selected areas. Typical acceleration voltages of 2 kV were applied. The samples were fixed on a conductive carbon tape and the polymeric sample surfaces have been sputter-coated with 5 nm of Au/Pd alloy to facilitate imaging.

To measure the peel strength of plasma-sputtered silver coatings on rPET and PET with different Ag film thicknesses (process conditions as given in Subjalearndee et al.<sup>[42]</sup>), an adhesive-tape peel test was performed according to ASTM D 3359. Tapes (2 cm wide) with different adhesion forces on the Ag layer have been used. The adhesion of the Ag-layer on the polymer samples can be considered to be higher than the adhesion force of the tape onto the Ag-layer as long as the Ag layer remains intact, whereas lower adhesion values result in film failure. Applying a tape with a maximum adhesion force of 26 N, a maximum adhesion of 13 N cm<sup>-1</sup> could be determined, exceeding the industrially relevant adhesion



value of  $\sim 10 \text{ N cm}^{-1}$ .<sup>[43]</sup> Note that the actually required adhesion force is typically defined by the end customer.

### 3 | RESULTS AND DISCUSSION

#### 3.1 | Selection of plasma etching conditions

A capacitively coupled asymmetric plasma reactor was used for plasma etching with different Ar/O<sub>2</sub> ratios at varying pressure and power input. The latter was limited to 30 W (driving voltage amplitude  $\sim 400 \text{ V}$ ) to avoid increased heat load within the reactor, whereby the gas temperature remains cold.<sup>[44]</sup> To optimize pressure, the luminosity distribution above the RF electrode was optically observed showing wider plasma zones, that is, increasing sheath width and plasma length, with reducing pressure (Figure 2). The luminosity indicates the formation of excited species in the plasma, which becomes increasingly asymmetric at higher pressure due to collisions.

By admixture of oxygen, the relative luminosity distribution varying with pressure remained unchanged. Etch rates were found to be rather comparable in the pressure range of 4–15 Pa (within 10% variation), while they noticeably dropped at lower pressures, indicating inverse effects of decreasing particle densities and increasing electron temperature and ion bombardment.

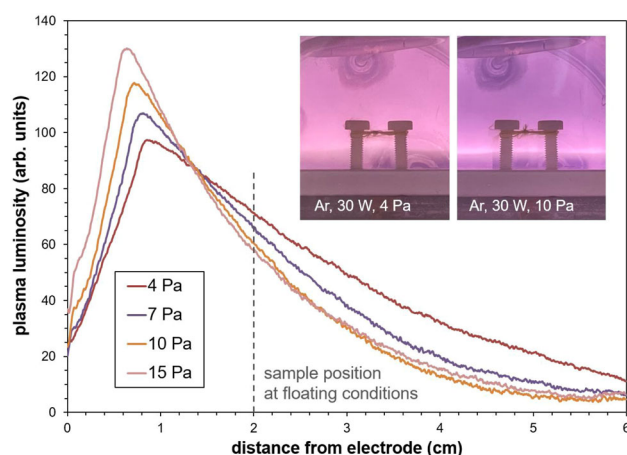


**FIGURE 2** Luminosity distribution in Ar plasma (30 W) for different pressures. The analyzed zone is confined by the electrode (left) and the gas inlet (right, 6 cm above the electrode). The maximum intensity indicates the sheath/plasma boundary, while the active plasma zone expands into the reactor volume, where the samples are placed 2 cm above the electrode. The inset pictures show the plasma expansion for two different pressures with the RF electrode at the bottom, the suspension system for samples at a floating potential, and the gas inlet ring at the top.

Hence, an optimum pressure of 4 Pa was selected to effectively immerse the samples in the active plasma zone, 2 cm above the electrode.

For this particular condition (Ar plasma, 30 W, 4 Pa), a negative bias potential of 350 V, an electron density of  $10^{10} \text{ cm}^{-3}$ , and an electron temperature of  $\sim 4 \text{ eV}$  were determined. From the latter, a voltage drop of around 20 V between plasma and floating potential can be deduced yielding ion energies of  $\sim 20 \text{ eV}$  (for a thin collisionless sheath), whereas at the electrode mean ion energies of  $\sim 140 \text{ eV}$  are present taking collisions into account.<sup>[45]</sup> Assuming comparable ion flux at the electrode and at floating potential, samples are thus exposed to a roughly seven times stronger ion bombardment, that is, energy flux, at the electrode, yielding increased etch rates and heat load, resulting in a substrate temperature of 80–120°C, depending on the gas. At floating potential milder conditions are present, where Ar ions of 20 eV still allow ion-induced chemical etching processes that can contribute to synergistic effects when O<sub>2</sub> is added.<sup>[46,47]</sup> These floating conditions enable a gas-independent substrate temperature of 65°C.

#### 3.2 | Melting and crystallization behavior of the examined polymers

The initial DSC heating curve, evaluated for plasma-treated PET, rPET, PP film, and injection-molded PP, describes the mechanical and thermal history of the as received and plasma-etched samples. The initial DSC heating curves of rPET are shown in Figure 3a. A glass transition temperature  $T_g$  of 75°C and a strong recrystallization peak at  $T_c = 135^\circ\text{C}$  were observed. The determined melting temperature  $T_m$  was 250°C, which is around 6°C lower compared with the virgin PET film (Figure 3c). This reduction in melting temperature can be an indication of shorter molecular chain lengths and heightened impurity content.<sup>[48]</sup> Since GPC detected a similar molecular weight of around 34 000 Da for the used rPET as also for virgin PET and an amorphous PET reference, the observed differences might be mainly due to contaminations and defects arising from the recycling process. For rPET, the melting enthalpy,  $\Delta H_m$ , was comparable to the cold-crystallization enthalpy ( $\Delta H_c$  at 135°C, see Table 1) and thus the resulting calculated crystallinity is small ( $\sim 10\%$ ). The WAXD pattern of rPET shows an amorphous ring (inset Figure 3a) and thus supports the DSC finding of low crystallinity. In comparison, virgin PET was found to be semi-crystalline with a calculated crystallinity of 31% and did not show any apparent exothermal recrystallization ( $\Delta H_c$ ) behavior. The film is stretched in a preferential

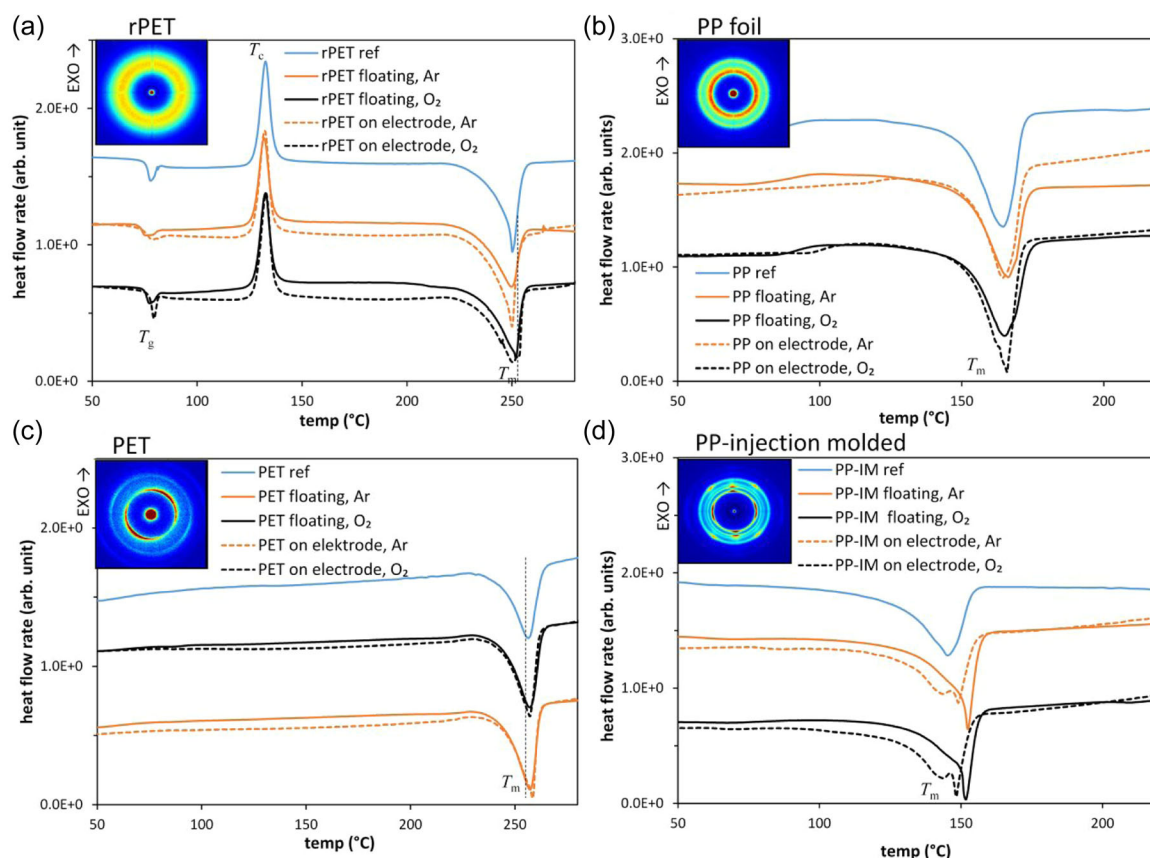


**FIGURE 3** Initial differential scanning calorimetry (DSC) heating curves of (a) recycled polyethylene terephthalate (rPET), (b) polypropylene (PP), (c) PET films, and (d) PP produced with injection molding technology etched with 30W for 7.5 min. Wide-angle x-ray diffraction (WAXD) patterns of untreated samples (ref) are shown as insets.

direction leading to a partially oriented crystalline structure as shown in the WAXD pattern for PET (see inset Figure 3c). Stretching the film as processed for PET films is often performed to gain stability and enhance transparency.<sup>[49]</sup>

The used plasma etching at floating conditions with 30 W (4 Pa, 7.5 min) did not induce changes to the PET and rPET bulk material properties as indicated by the retained form of the DSC curves and the unchanged crystallization values shown in Table 1. Only the rPET polymer, with low initial crystallinity, shows a 3% absolute increase in crystallinity as a result of the treatment conditions directly at the electrode yielding increased heat load. For comparison, an rPET sample was annealed in the oven at 160°C for 10 min and achieved a crystallinity of 27%, losing transparency and mechanical flexibility.

For PP the DSC and WAXD results are shown in Figure 3b,d. The glass transition temperature  $T_g$  of PP lies between  $-18^{\circ}\text{C}$  and  $0^{\circ}\text{C}$ , which is outside the range of the diagram. The PP film (Figure 3b) is for a large part crystalline ( $\sim 35\%$ ) and the WAXD pattern shows that the crystals are not oriented. In contrast,

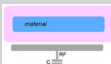
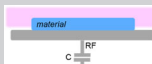
the injection molded PP sample exhibited a comparable crystallinity of 34% but has highly oriented crystals. During injection molding, PP is pressed within milliseconds into a cold mold, whereby the flow of the polymer melt follows a so-called fountain flow (entering in the center and turning toward the wall at the melt front), which strongly affects the microstructure of the injection-molded material. Investigations from Moneken show that the first material in contact with the mold forms a thin amorphous skin layer due to the high cooling rate.<sup>[50]</sup> The following polymer material encounters a smaller cooling rate and can thus crystallize forming the well-oriented crystalline layer below the top skin layer.<sup>[51]</sup> The outermost amorphous skin layer of the etched injection-molded polymer (Figure 4) is very sensitive to the etchants as we will discuss in the following sections. Additionally, SEM images of untreated or etched samples (PET, rPET, PP, and PP-IM) are discussed in Section 3.6.

However, the mild plasma etching of both PP types treated under floating conditions did not significantly alter the bulk crystallinity (see Table 1), which is

**TABLE 1** Cold-crystallization enthalpy  $\Delta H_c$ , melting enthalpy  $\Delta H_m$ , calculated degree of crystallinity  $W_c$  (bold), crystallization Temperature  $T_c$  and melting Temperature  $T_m$  for untreated, Ar and  $O_2$  plasma-etched polymers on floating and on electrode potential

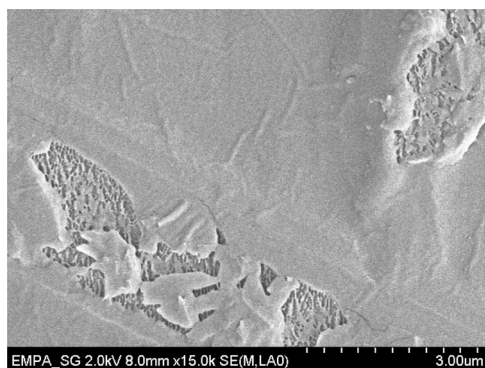
REF °C	$\Delta H_c$ (Jg <sup>-1</sup> ) $T_m$ °C	$\Delta H_m$ (Jg <sup>-1</sup> )	$W_c$	$T_c$	
PET	0	43.2	<b>31%</b>	-	256
rPET	27.3	42.3	<b>11%</b>	133	250
PP	17.1	88.7	<b>35%</b>	60–135	165
PP IM	0	71.3	<b>34%</b>	-	145

floating 						on electrode 				
PLASMA	$\Delta H_c$ (Jg <sup>-1</sup> )	$\Delta H_m$ (Jg <sup>-1</sup> )	$W_c$	$T_c$ °C	$T_m$ °C	$\Delta H_c$ (Jg <sup>-1</sup> )	$\Delta H_m$ (Jg <sup>-1</sup> )	$W_c$	$T_c$ °C	$T_m$ °C
PET/ $O_2$	0	44.7	<b>32%</b>	-	257	0	43.9	<b>31%</b>	-	257
PET/Ar	0	43.8	<b>31%</b>	-	257	0	43.7	<b>31%</b>	-	258
rPET/ $O_2$	24.8	39.3	<b>10%</b>	132.5	252	26.8	46.8	<b>14%</b>	133	251
rPET/Ar	23.7	35.9	<b>9%</b>	131.9	245	27.2	45.1	<b>13%</b>	132	250
PP/ $O_2$	10.9	77.1	<b>32%</b>	60–135	165	7.5	87.3	<b>39%</b>	60–135	166
PP/Ar	13.3	72.3	<b>29%</b>	60–135	169	0.6	81.8	<b>39%</b>	60–135	164
PP-IM/ $O_2$	0	62.3	<b>30%</b>	-	152	0	79.8	<b>39%</b>	-	148
PP-IM/Ar	0	68.6	<b>33%</b>	-	152	0	71.8	<b>35%</b>	-	149

Note: PET, rPET, and PP are films and PP-IM is an injection-molded PP. Standard deviation of the crystallinity is calculated to  $\pm 1\%$  by varying the integration boundaries by  $\pm 1.5^\circ\text{C}$  to the normal.

Abbreviations: PET, polyethylene terephthalate; PP, polypropylene; rPET, recycled PET.



**FIGURE 4** Amorphous surface skin layer, hundreds of nanometer thick, of the injection-molded polypropylene (PP-IM) sample after plasma etching (floating, 30 W, 1/19 sccm Ar/ $O_2$  flow, 7.5 min). Scratches reveal the semi-crystalline, spherulitic phases underneath.

expected since the etching is only removing part of the top surface layer (less than 500 nm). In contrast, PP samples plasma etched on the electrode show at the same plasma conditions an absolute increase in crystallinity of up to 7% due to the induced higher heat load.

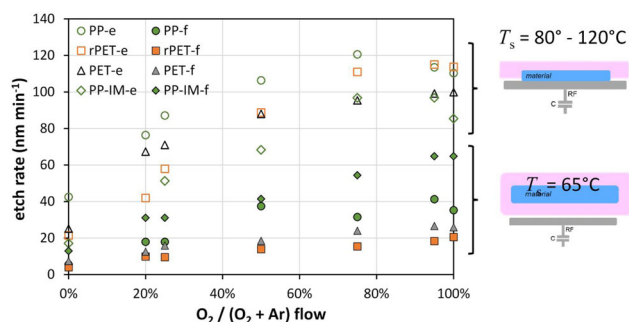


**FIGURE 5** Averaged etch rates for increasing  $O_2$  flow for two setups; samples at floating conditions, 2 cm above the radio frequency (RF) electrode (denominated by “-f”, e.g., PET-f), and samples placed at the electrode (denominated by “-e”). The plasma conditions were: total flow of 20 sccm, 30 W, 4 Pa, 7.5 min with a sample size of 135 cm<sup>2</sup>, that is, the sample is almost as large as the RF electrode of 150 cm<sup>2</sup>. The standard deviation of  $\pm 3.1$  nm min<sup>-1</sup> (PET) and  $\pm 2.1$  nm min<sup>-1</sup> (PP) is not shown for ease of reading. PET, polyethylene terephthalate; PP, polypropylene.

### 3.3 | Reactive gas-dependent etch rate

Figure 5 presents the etch rates for PET, rPET, PP films, and injection-molded PP with varying Ar/ $O_2$  ratios in the plasma.

The total flow rate was kept at 20 sccm (30 W, 4 Pa), while the oxygen flow rate was increased. Samples on the electrode are denominated by “-e” and floating samples are denominated by “-f”. Samples placed at the electrode resulted in higher etch rates for all polymers due to higher ion energies. Higher ion energies are associated with higher measured sample temperatures  $T_S$ . For etching with pure  $O_2$ ,  $T_S$  was 80°C, while for Ar,  $T_S$  around 120°C was measured at the electrode. As shown in Table 1, rPET and PET have 11% and 31% crystallinity, respectively. For plasma etching performed on the electrode (and thus above  $T_g$ ), with increased crystallinity, for example, PET-e, is accompanied by a decrease in etch rate compared with rPET-e. This finding could also be proved with the oven-treated rPET samples (annealed crystallinity of 27%) which resulted in a lower etch rate. The high ion energy favors the preferential etching of the amorphous areas.

The PP and PP-IM samples treated on the electrode showed different etch rates despite similar crystallinity. In this case, attention must be paid to the film thickness. On the electrode, injection molded PP-e showed the lowest etch rates among the examined polymer samples, likely due to the thicker substrate of 600  $\mu\text{m}$  affecting surface charging and thus ion bombardment.<sup>[52]</sup>

Due to the asymmetric set-up with stronger ion bombardment at the RF electrode (as discussed above), the lowered ion energies at a floating potential, lead to a lower substrate temperature  $T_S = 65^\circ\text{C}$  for both process gases. The observed etch rates at floating potential were roughly two to three times lower but still around 10  $\text{nm min}^{-1}$  for pure Ar plasma, which were noticeably enhanced by oxygen admixture (up to five to six times). The highest etch rate at floating potential was found for the injection-molded PP-IM-f followed by the PP-f and virgin PET-f, whereas slightly lower etch rates were observed for the rPET-f film despite its lower crystallinity. To verify this trend, rPET was annealed at 160°C to enhance its crystallinity to be comparable to the used virgin PET. Indeed, an increased etch rate even higher than for the virgin material was observed (not shown). Hence, processing temperature with respect to  $T_g$  is a crucial factor for polymer processing including plasma treatment, while basic differences between recycled and virgin polymers such as embedded impurities and defects (as indicated by the lower melting point of rPET by DSC) need to be considered, as well.

Studies referring to the Onishi parameter predict a higher etch rate for O-containing polymers such as PET compared with PP. Note again that the polymer samples here were treated with mild plasma conditions at floating potential (limited ion energy of 20 eV) resulting in low  $T_S$  distinctly staying below 70°C for Ar and  $O_2$  during the plasma etching process. In these conditions, PP-f and PP-e were treated at temperatures above their  $T_g$ , whereas PET-f

was treated below its  $T_g$  of around 75°C which can lead to differences in etch rates. Polymers above the glass transition temperature show soft mechanical properties with enhanced elasticity because of higher chain mobility supporting increased etch rates.<sup>[30]</sup>

In comparison, PET-f films as treated below  $T_g$  have lower chain mobility and are more brittle, explaining the lower etch rate compared with PP-f. These findings were also observed by Krstulovic.<sup>[31]</sup> Etch rates of PET under these mild floating conditions can also be increased by  $O_2$  addition but generally at a lower level than treatments on the electrode. On the contrary, plasma-etched PET with 200 eV Ar ions, that is, 10-fold higher than here, already showed high etch rates in pure Ar that were not further enhanced by oxygen admixture.<sup>[47]</sup> We thus assume that thermal effects at the polymer surface are responsible for the observed differences and thus need to be taken into account for polymer etching processes.

Finally, the higher etch rate of injection-molded PP-IM-f compared with the PP-f film can be explained by the fact that the injection-molded PP samples have an amorphous skin layer and overall slightly lower bulk crystallinity compared with the PP film (Table 1). The amorphous PP skin on the crystalline PP phase can clearly be seen in Figure 4 which is fully exposed to the plasma etch species yielding a higher etch rate than the semi-crystalline region underneath. For substrates etched under floating conditions, it should be noted that the etch rate is less dependent on the film thickness.

### 3.4 | Sample surface area-dependent etch rate

Plasma processing of polymer films, foils, fibers or 3D objects using capacitively coupled plasmas comprise an electrode covering a defined area. For etching processes applied directly on the RF electrode, for example, for wafer processing, the electrode size typically corresponds to the sample size. For samples treated in the active plasma zone at a floating potential, various options can be selected in terms of sample size and treated area, for example, the front and backside of a foil can be intentionally treated the same way or differently. To this end, the influence of the sample size was studied by performing the same reactive plasma etching ( $O_2$  plasma, 30 W, 4 Pa, 7.5 min) with different sample sizes at floating conditions shown in Figure 6. Since the used RF electrode area was defined to 150  $\text{cm}^2$ , we generalize the sample size relative to the electrode area.

For small sample areas, where the sample to electrode ratio approaches zero, such as fibers and narrow ribbons, the etch rates appeared to be homogeneous, that is, with 50% on top and 50% on the bottom side of the sample. With



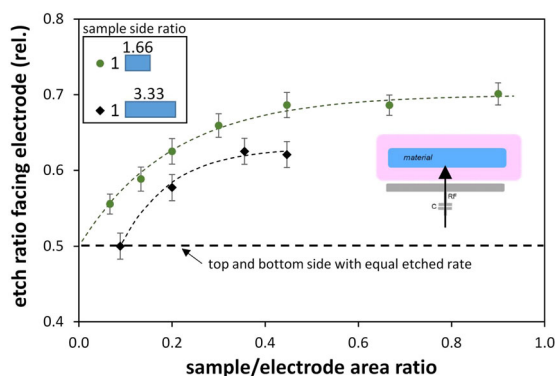


**FIGURE 6** Relative etch rates at floating conditions by plotting the etch rate on the side facing the electrode relative to the total etch rate (top and bottom side of the two films). Electrode size  $150\text{ cm}^2$ , 4 Pa, 20 sccm  $\text{O}_2$ , 30 W, 7.5 min, sample floating 2 cm above electrode. Dashed line drawn to guide the reader's eye. The width of the standard deviation is displayed at  $\pm 2.1\text{ nm/min}$ .

increasing sample size the surface facing the electrode underwent an increasingly stronger etching effect, while the total etch rate was largely maintained. The increasing sample size is acting to confine the plasma between the electrode and the floating sample. In this sense, a narrower sample (aspect ratio 1:3.33 in Figure 6), reached an equal etch rate on the top and bottom side at the sample size of  $2 \times 6.6\text{ cm}^2$  (ratio = 0.09). These findings could be used similar to a two-sided treatment of a polymer film in an industrial R2R process. In this way, the plasma can better enclose the sample supported by a mean free path length of  $\sim 1\text{ cm}$ , resulting in a more uniform etch rate on the top and bottom sides.

### 3.5 | Time-dependent etch rate

For the third experimental series, the influence of the plasma etching duration on the etch rate was studied for two-sided treatments. For this purpose, elongated samples with a ratio of  $3 \times 10\text{ cm}^2$  were used with almost identical etching conditions of the top and bottom surfaces according to the results in Figure 6. The same polymer samples were repeatedly treated with  $\text{Ar}/\text{O}_2$  (1:19 sccm) plasma process for a total etching time of 60 min. Between each process, the vacuum chamber was opened and the samples were weighed to determine the time-dependent etch rate. The normalized etch rate was decreased by continuing the experiment as can be seen in Figure 7. A lower etch rate over time has also been reported in the literature.<sup>[25,53]</sup> The results of Fernandez et al. have been associated with morphological changes (i.e., reorganization) occurring in the samples when they approach their thermal transition temperatures as a consequence of the temperature increase at the electrode

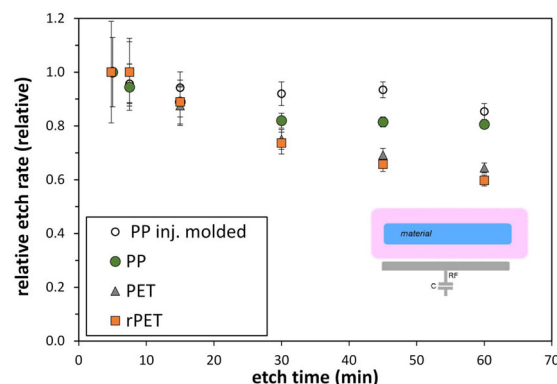


**FIGURE 7** Time-dependent etch rates for polyethylene terephthalate (PET), recycled PET (rPET), polypropylene (PP) films, and injection-molded PP- treated with different plasma etching times. All samples were placed at floating condition 2 cm above the electrode with plasma treatment of 30 W, 4 Pa,  $\text{Ar}/\text{O}_2$  flow 1/19 sccm.

during treatment. In addition, plasma surface interactions lead to a competition between chain scission and cross-linking, distinctly for Ar, He, or  $\text{N}_2$ , in the near-surface layer that can result in a reduced etch rate over time.<sup>[54]</sup> Furthermore, for longer treatment times of plasma-polymer interaction, an effect by vacuum ultraviolet (VUV) radiation becomes more significant yielding free radical to a depth of  $1\text{--}2\text{ }\mu\text{m}$ , whereas for shorter etching ( $t < 30\text{ min}$ ) a low contribution of VUV ( $140\text{--}155\text{ nm}$ ) has been observed.<sup>[54,55]</sup>

In principle, also a sputtering effect from the electrode made of aluminum could yield a reducing etch rate at floating conditions over time. Tsougeni et al.<sup>[22]</sup> identified alumina on plasma-etched polymer samples for higher power regimes. These particles, which are nonvolatile, redeposit on the nearby surface including the polymer samples, where they act as micromasks causing locally different etch rates and promoting the development of column-like structures. The amount and composition of the aluminum contamination might also vary with the history of the plasma reactor.<sup>[22]</sup> Applying the rather mild plasma etching conditions (30 W, 4 Pa) for 1 h with  $\text{Ar}/\text{O}_2$  (19:1), however, resulted in only low aluminum concentrations (0.3 wt% as determined by X-ray photoelectron spectroscopy (XPS)) on the polymer sample surfaces facing the electrode.

### 3.6 | Morphology of etched polymer surfaces

Figure 8 displays the untreated sample surfaces before plasma treatment using SEM images. PET, rPET, and PP polymer films ( $3 \times 10\text{ cm}^2$ ) were then plasma-treated at floating potential and directly on the RF electrode

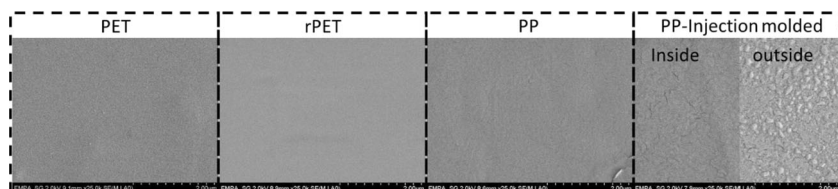


**FIGURE 8** Surface morphology of untreated polymer samples shown as a reference

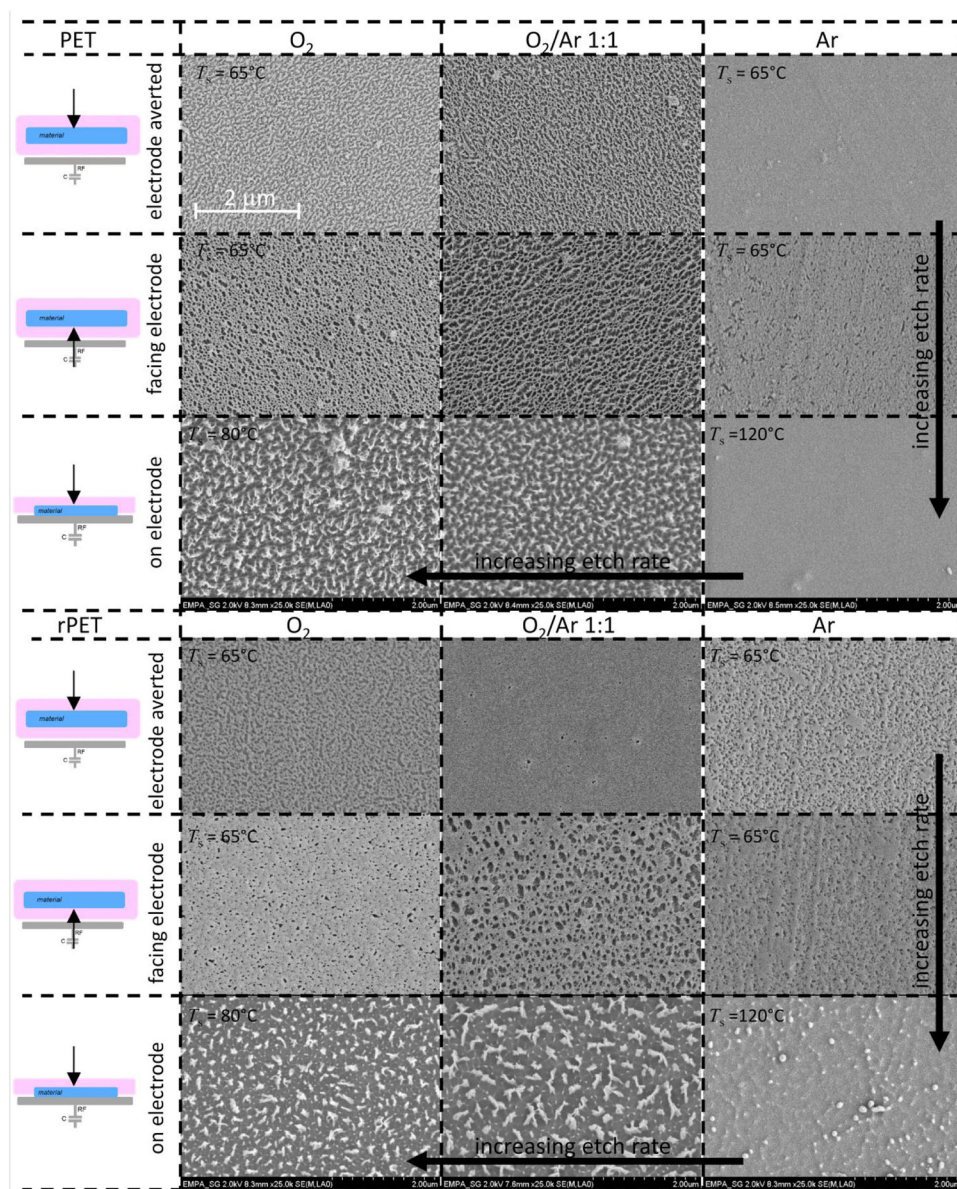


**FIGURE 9** Scanning electron microscopy (SEM) images of polyethylene terephthalate (PET) (top ensemble) and recycled polyethylene terephthalate (rPET) films (lower ensemble) that were plasma etched (30W, 4 Pa, and 7.5 min) with the gas flow conditions indicated per column. Samples were placed at floating conditions analyzing the top and bottom side as well as on the radiofrequency (RF) electrode thus exposed to different ion bombardment.

( $5 \times 15 \text{ cm}^2$ ). The injection-molded PP cup showed differences in surface morphology of the inner and outer surfaces originating from the mold. Therefore, the more uniform inner surface was investigated.

SEM images of the etched polymer samples are presented in Figure 9, arranged to have an increasing

etch rate from upper right to lower left, as indicated by the arrows for each set of data, in the order from low to high etch rates for gas conditions (Ar to Ar/O<sub>2</sub> 1:1 to O<sub>2</sub>) according to Figure 5. Samples have been located at three different positions in the plasma: floating (top and bottom side) and on the electrode.



The morphology of PET and rPET opposite to the electrode (top row in Figure 9) revealed a smoother etching compared with the sample side facing the electrode. This could be a consequence of the ion bombardment, for example, lower etching rate on the top surface with  $54 \text{ nm min}^{-1}$  compared with  $68 \text{ nm min}^{-1}$  on the bottom side. The more crystalline and oriented virgin PET evolved a clear surface structure, whereas the amorphous rPET showed less pronounced structures. The polymer film facing the electrode (second row) exhibits predominantly voids within a fine network of fibrillary structures on both PET and rPET surfaces. The subtractive effect and sharpened edges are more pronounced for the

crystalline-oriented PET. In contrast, the fibrillar network is more distinctive for rPET and the etched void-like structures cover less surface area. The samples etched on the electrode show columnar structures of inherent polymer material, which might well correlate with the different crystallinity of the two PET polymers. Pure Ar plasma treatment resulted in little or no surface structure which is known from the atom by atom removal at physical etching conditions.

Plasma etching of injection-molded PP led to a very regular and smooth removal of the polymer material under all conditions (Figure 10, top ensemble). No structures or patterns can be seen in the SEM

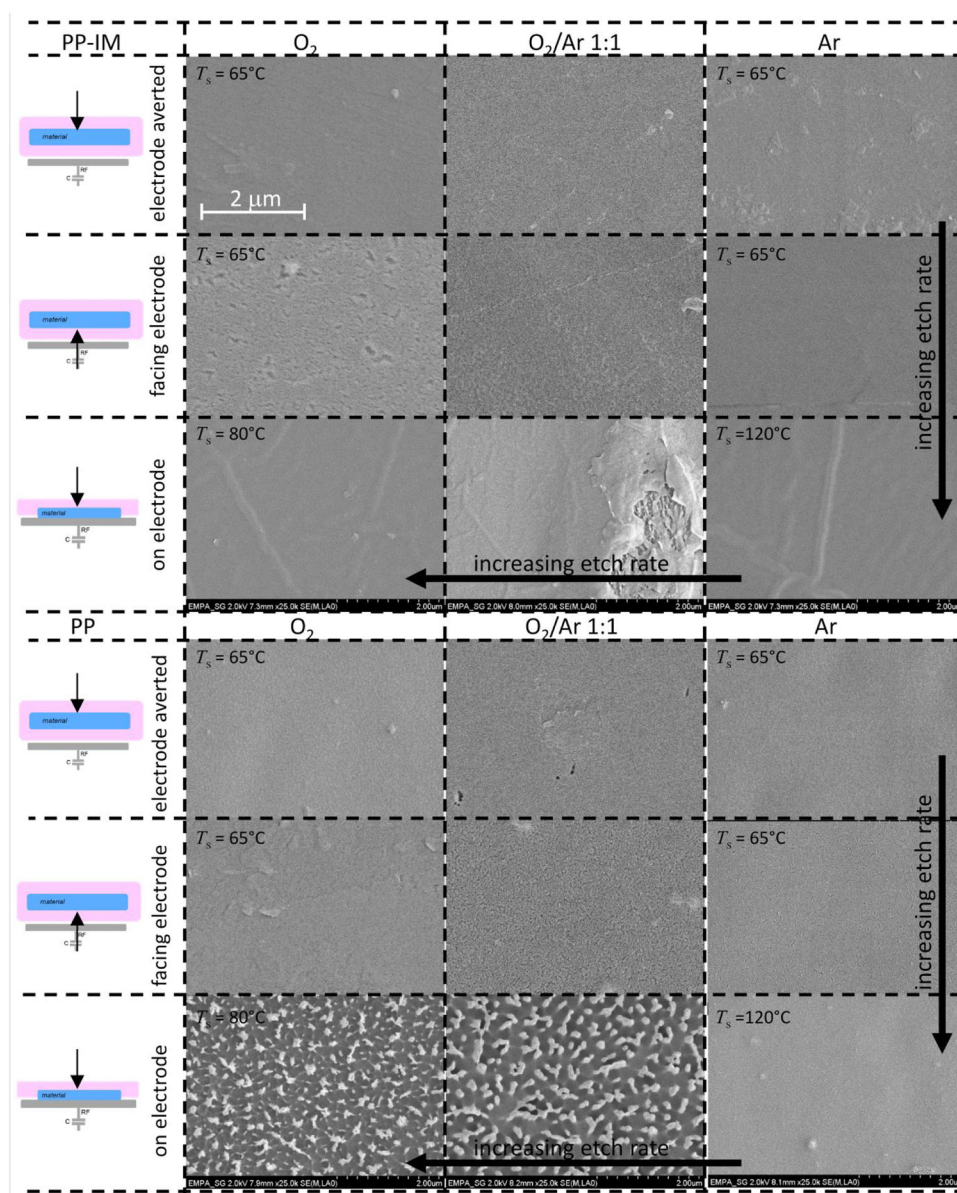


**FIGURE 10** Scanning electron microscopy (SEM) images of injection-molded polypropylene (PP) (top ensemble) and PP film (lower ensemble) that were plasma etched with the same conditions as specified in Figure 9

investigations in Figure 10 (first two rows) due to the low energy conditions of the floating plasma.

For the PP film shown in the lower ensemble, etching structures became visible for samples treated on the electrode with oxygen admixture, where the synergistic effect of higher energy particles predominates. Ar plasma treatment takes advantage of the absence of reactive oxygen species while providing a more efficient energy transfer due to the heavy ions incident on the sample surface. This argon ion bombardment (physical etching) homogeneously removes amorphous as well as crystalline domains, resulting in smooth surfaces independent of the sample placement.

### 3.7 | Adhesion of Ag coatings on plasma-etched recycled PET

Silver layers with varying thicknesses of around 50, 150, and 350 nm were deposited on plasma-treated PET and rPET films using dc magnetron sputtering. This way, plasma etching at floating potential as discussed before was applied to improve the adhesion of Ag coatings onto the polymer side facing the RF electrode. An adhesive-tape peel test was used to determine adhesion strength. Importantly, high adhesion forces exceeding  $13 \text{ N cm}^{-1}$  could be achieved on both virgin and recycled PET when applying rather mild etching conditions with Ar/O<sub>2</sub> plasmas (Figure 11). Due to the limited adhesion of the used tape on silver, possible differences between rPET and PET were not further assessed. For comparison, a peel strength up to  $40 \text{ N cm}^{-1}$  was reported for electroless deposited Ag on thiol-modified PET surfaces, while lower values around  $4 \text{ N cm}^{-1}$  are typically observed for

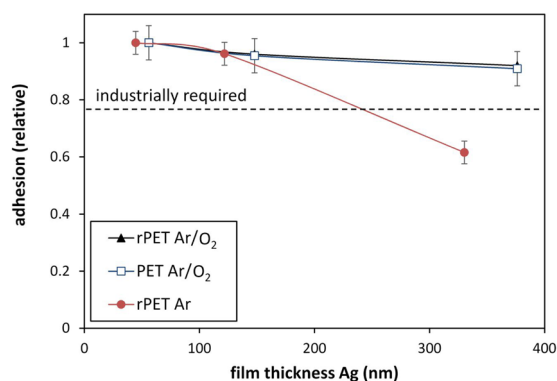


**FIGURE 11** Adhesion forces of sputtered silver coatings on virgin and recycled polyethylene terephthalate (PET) films for plasma etching processes with Ar and Ar/O<sub>2</sub> (1:1) gas mixtures. Peel strength of  $>10 \text{ N cm}^{-1}$  was defined for the intended application (indicated by the dashed line).

silver evaporation.<sup>[56]</sup> Reduced adhesion strength and film failure could only be detected for thicker Ag coatings on Ar plasma-treated rPET. Hence, plasma chemical etching was found to be well suited to treat recycled polymer material despite different mechanical and morphological properties when compared with virgin PET. The obtained adhesion strength was sufficient to enable R2R processing for metallization and subsequent deep drawing of the metallized rPET film by thermoforming as used for highly insulating container wall structures that reflect 96% of heat radiation already with a 50 nm thick metal coating.

## 4 | CONCLUSION

The characteristics of recycled PET in plasma etching processes have been studied by applying mild plasma conditions at the floating potential to limit heat load. The plasma-treated rPET films using different Ar/O<sub>2</sub> gas mixtures were compared with virgin PET and PP films as well as injection-molded PP based on sample temperature, etch rate, morphology, and thermal analysis techniques.

The plasma treatment at floating conditions maintained sample temperatures below 65°C, that is, below the glass transition temperature of the used material, regardless of the process gas used, which had no effect on the bulk crystallinity of any of the polymers studied. Comparison with polymer samples treated on the electrode at the same plasma conditions, on the contrary, revealed a relative increase in crystallinity for all polymer types due to the higher ion energies incident on the electrode, yielding higher sample temperatures. The highest relative increase was observed for the initially least crystalline rPET, that is, from 9%–10% to 13%–14%. Note that comparative heat treatment in an oven resulted in a crystallinity increase of up to 27%. The substrate temperature during plasma etching can thus become a crucial factor.

The etch rate of rPET at floating potential was found to be slightly lower compared with virgin PET despite the lower crystallinity of rPET, revealing important basic differences between etching on the RF electrode and at floating. This result might be unexpected since higher etch rates have generally been reported for less crystalline surfaces. The differences in etch rate might thus be related to the combination of low ion energy etching at temperatures below the material's  $T_g$ , where chemical etching is preferential. The additional impact might be related to embedded impurities and defects of rPET, which was reflected by the lower melting point by DSC, while molecular weights were found to be comparable.



Despite those differences, plasma etching conditions with Ar/O<sub>2</sub> mixtures at low pressure, inducing low heat load (below  $T_g$ ), were found to yield suitable morphologies as studied by SEM to promote adhesion. To this end, the adhesion improvement of silver coatings on rPET after plasma etching could be demonstrated to yield comparable adhesion strength to virgin PET independent of small differences in morphology (and crystallinity). These findings are important for industrial processing of recycled PET material to meet quality requirements, for example, to produce sustainable nano-coated, heat-reflecting containers for the transport of goods at maintained low temperatures. Metalized polymer films are lighter and have a significantly higher mechanical resistance compared with metal foils.

Experiments with different sample sizes indicated that for very small samples such as yarns, the etch rate under floating conditions was the same on the bottom as on the top side. For industrial, two-sided film treatment, an elongated sample size with a factor of 0.25 of the electrode size showed a treatment ratio of 56% on the bottom and 44% on the top side. Thus, industrial two-sided R2R plasma treatment would also be possible in one run, emphasizing the virtues of plasma etching in floating conditions beside reduced heat load.

This study addresses the topic of transparent polymers without color additives. The diversity of recycling methods and polymer precursors leads to many different polymer recyclates and properties that need to be researched and classified in the future.

## ACKNOWLEDGMENTS

Mathias Lienhard and Rolf Widmer are greatly acknowledged for their profound discussion about recycled materials. Tomas Plichta and Milan Mihajlovic are greatly acknowledged for their well-founded contribution to sample treatments in the lab. M. Amberg and D. Hegemann acknowledge funding by Innosuisse—the Swiss Innovation Agency, Grant/Award Number: 12404.1 PFIW-IW. Open access funding provided by ETH-Bereich Forschungsanstalten.

## CONFLICT OF INTEREST

The authors declare no conflict of interest.

## DATA AVAILABILITY STATEMENT

Data available on request from the authors.

## ORCID

Martin Amberg  <http://orcid.org/0000-0002-8900-8636>

Dirk Hegemann  <http://orcid.org/0000-0003-4226-9326>

## REFERENCES

- [1] C. M. Weikart, H. K. Yasuda, *J. Polym. Sci., Polym. Chem. Ed.* **2000**, 38, 3028.
- [2] G. S. Oehrlein, R. J. Phaneuf, D. B. Graves, *J. Vac. Sci. Technol. B* **2011**, 29, 010801.
- [3] M. Klotz, M. Haupt, S. Hellweg, *Waste. Manag.* **2022**, 141, 251.
- [4] C. Meran, O. Ozturk, M. Yuksel, *Mater. Design* **2008**, 29, 701.
- [5] K. Wang, F. Addiego, S. Ahzia, Y. Rémonda, V. Toniazio, *Comp. Sci. Technol.* **2014**, 95, 89.
- [6] P. S. Garcia, C. H. Scuracchio, S. A. Cruz, *Polym. Testing* **2013**, 32, 1237.
- [7] İ. Özkan, S. Gündoğdu, *J. Text. Inst.* **2021**, 112(2), 264.
- [8] T. Felix, V. Soldi, N. A. Debacher *Plasma Modification of Polyolefins* (Eds: N. S. Baneesh et al.), Springer Nature Switzerland AG, Cham, Switzerland, **2022**, pp. 197.
- [9] S. A. Cruz, M. Zanin, P. A. P. Nascente, M. A. Bica de Moraes, *J. Appl. Polym. Sci.* **2010**, 115, 2728.
- [10] S. M. D. Prestes, S. D. Mancini, E. C. Rangel, N. Cristino da Cruz, W. H. Schreiner, A. R. Junior, *Plasma. Process. Polym.* **2015**, 12, 456.
- [11] T. Hirotsu, K. Qi, K. Nakayama, *Polym. Polym. Composites* **2004**, 12, 689.
- [12] S. M. Irvin, *Proc. Kodak Photoresist Seminar* **1968**, 2, 26.
- [13] F. D. Egitto, V. Vukanovic, G. N. Taylor *In Plasma Deposition, Treatment, and Etching of Polymers*, (Ed: R. d'Agostin), Academic Press, Boston, USA, **1990**. Ch. 5.
- [14] F. D. Egitto, L. J. Matienzo, *IBM J. Res. Dev.* **1994**, 38, 423.
- [15] R. M. France, R. D. J. Short, *Chem. Soc. Faraday Trans.* **1997**, 93, 3173.
- [16] F. Denes, *Trends Polym. Sci.* **1997**, 5, 23.
- [17] B. D. Beake, J. S. Ling, G. J. Leggett, *J. Mater. Chem.* **1998**, 8, 1735.
- [18] J. A. G. Baggermann, R. J. Visser, E. J. H. Collart, *J. App. Phys.* **1994**, 75, 758.
- [19] S. L. Kaplan, P. W. Rose, *Int. J. Adhes. Adhes.* **1991**, 11, 109.
- [20] M. M. Hossain, D. Hegemann, A. S. Herrmann, P. Chabreck, *J. Appl. Polym. Sci.* **2006**, 102, 1452.
- [21] N. Inagaki, K. Narushim, N. Tuchida, K. Miyazaki, *J. Polym. Sci. B Polym. Phys.* **2004**, 42, 3727.
- [22] K. Tsougeni, A. Tserepi, G. Boulousis, V. Constantoudis, E. Gogolides, *Jap. J. Appl. Phys.* **2007**, 46, 744.
- [23] O. Kylián, J. Benedikt, L. Sirghi, R. Reuter, H. Rauscher, A. von Keudell, F. Rossi, *Plasma. Process. Polym.* **2009**, 6, 255.
- [24] G. D. Bourceanu, M. D. Gheorghiu, C. Moisa, *Rev. Roum. Phys.* **1985**, 30, 145.
- [25] J. P. Fernandez-Blázquez, A. del Campo, *Soft Matter* **2012**, 8, 2503.
- [26] J. Meichsner, M. Nitschke, R. Rochotzki, M. Zeuner, *Surf. Coat. Technol.* **1995**, 74-75, 227.
- [27] H.-S. Ko, J.-W. Nah, K. W. Paik, Y. Park, *J. Vac. Sci. Technol. B* **2002**, 20, 1000.
- [28] A. Vesel, T. Semenik, *Mater. Technol.* **2012**, 46, 3.
- [29] L. Xie, Q. L. Dai, G. Du, Q. Deng, G. Liu, *Appl. Mech. Mater.* **2012**, 200, 194.
- [30] M. Pons, O. Joubert, P. Paniez, J. Pelletier, *J. Appl. Phys.* **1991**, 70, 237.

- [31] N. Krstulovic, I. Labazan, S. Milošević, U. Cvelbar, A. Vesel, M. Mozetič, *J. Phys. D Appl. Phys.* **2006**, *39*, 3799.
- [32] G. Fischer, A. Haemeyer, J. Dembowski, H. Hibst, *J. Technol.* **1994**, *8*, 151.
- [33] H. M. Powell, J. J. Lannutti, *Langmuir* **2003**, *19*, 9071.
- [34] L. Holland, S. M. Ojha, *Vacuum* **1976**, *26*, 53.
- [35] J. Trieschmann, D. Hegemann, *J. Phys. D Appl. Phys.* **2011**, *44*, 475201.
- [36] M. A. Keller, G. Fortunato, E. Körner, D. Hegemann, *Plasma. Process. Polym.* **2007**, *4*, 1063.
- [37] K. Holmberg, D. O. Shah, M. J. Schuger, *Handbook of Applied Surface and Colloid Chemistry*, John Wiley, New York **2002**.
- [38] D. Hegemann, U. Schütz, *Thin Solid Films* **2005**, *491*, 96.
- [39] D. Hegemann, *Thin Solid Films* **2006**, *515*, 2173.
- [40] G. Oder, *Structural Investigations of Polymers*, Ellis Horwood, New York **1991**.
- [41] A. van der Wal, J. J. Mulder, R. J. Gaymans, *Polymer* **1998**, *39*, 5477.
- [42] N. Subjalearddee, D. Hegemann, M. Amberg, B. Hanselmann, P. Rupper, V. Intasanta, *Appl. Surf. Sci.* **2018**, *452*, 306.
- [43] H. Kupfer, G. K. Wolf, *Nucl. Instr. Meth. Phys. Res. B* **2000**, *166–167*, 722.
- [44] D. A. Schulenberg, I. Korolov, Z. Donko, A. Derzsi, J. Schulze, *Plasma Sources Sci. Technol.* **2021**, *30*, 105003.
- [45] A. Manenschijn, W. J. Goedheer, *J. Appl. Phys.* **1991**, *69*, 2923.
- [46] T. A. R. Hansen, J. W. Weber, P. G. J. Colsters, D. M. H. G. Mestrom, M. C. M. van de Sanden, R. Engeln, *J. Appl. Phys.* **2012**, *112*, 013302.
- [47] A. von Keudell, C. Corbella, *J. Vac. Sci. Technol. A* **2017**, *35*, 050801.
- [48] E. Bormashenko, G. Whyman, V. Multanen, E. Shulzinger, G. Chaniel, *J. Coll. Interface Sci.* **2015**, *448*, 175.
- [49] M. E. Brown (eds). Purity determination using DSC. Introduction to thermal analysis. Hot topics in thermal analysis and calorimetry, vol. 1, Springer, Dordrecht. **2004**. [https://doi.org/10.1007/0-306-48404-8\\_11](https://doi.org/10.1007/0-306-48404-8_11)
- [50] M. T. De Meuse, *Biaxial Stretching of Film: Principles and Applications*, Elsevier, Amsterdam, Netherland, **2011**.
- [51] M. Moneke Ph.D. thesis, Die Kristallisation von verstärkten Thermoplasten während der schnellen Abkühlung und Unter Druck, Technische Universität Darmstadt (Darmstadt, Germany) 2001.
- [52] F. Liu, C. Guo, X. Wu, X. Qian, H. Liu, J. Zhang, *Polym. Adv. Technol.* **2012**, *23*, 686.
- [53] D. Hegemann, H. Brunner, C. Oehr, *Nucl. Instrum. Methods. Phys. Res. B* **2003**, *208*, 281.
- [54] A. C. Fozza, J. E. Klemberg-Sapieha, M. R. Wertheimer, *Plasmas Polym.* **1999**, *4*, 183.
- [55] A. N. Ponmarev, V. N. Vasilets, R. V. Talrose, *Chem. Phys.* **2002**, *21*, 96.
- [56] Y. Lu, S. Jiang, Y. Huang, *Synth. Met.* **2010**, *160*, 419.

**How to cite this article:** M. Amberg, M. Höhener, P. Rupper, B. Hanselmann, R. Hufenus, S. Lehner, E. Perret, D. Hegemann, *Plasma Processes Polym.* **2022**;19:e2200068. <https://doi.org/10.1002/ppap.202200068>